Comparative analysis of classical models (Mars3d, Azov3d) and Lattice Boltzmann models for shallow water hydrodynamics computations

A.I. SUKHINOV[a], E.V. ALEXEENKO[a], B.V. SIDORENKO[a], A.E. CHISTYAKOV[a], F. DUMAS[b], S. THEETTEN[b]

a. *Taganrog Institute of Technology, 44 Nekrasovsky str.; 347928 Taganrog (Russa)*
b. N DYNECO/PHYSED, IFREMER-Brest ; BP 70; 29280 Plouzané (France)

Résumé :

Différentes approches numériques de l'hydrodynamique de bassins en eau peu profonde sont considérées et comparées. Deux des approches ont été développées par le TIT : l'une d'elle est basée sur la résolution numérique des équations de Navier-Stokes avec correction de pression, l'autre (développée il y a plusieurs années) est basée sur la résolution numérique de l'équation de Boltzmann sur réseau. L'analyse comparative de ces deux approches a été faite avec MARS3D dans le cas d'un bassin en eau peu profonde : l'Etang de Berre.

Abstract :

Different numerical approaches of hydrodynamics of shallow water basins are considered and compared. Two approaches are developped in TIT-Russia: one of them is classical and based on numerical solution of the Navier-Stokes equations by Pressure-Correction method, another (developed several years ago) is based on the solution of the Lattice Boltzmann kinetic equation. The comparative analysis of these two approaches with MARS3D is performed for a shallow water basin example: «Etang de Berre».

keywords: shallow water hydrodynamics

Introduction

For the numerical simulation of hydrodynamics of shallow water basins different approaches are considered and compared. Two of them are developed in TIT-Russia: one is classicaly based on numerical solution of the Navier-Stokes equations by Pressure-Correction method, another (developed several years ago) is based on the solution of the Lattice Boltzmann kinetic equation, which is higher in the hierarchy of models. The comparative analysis of these two approaches with MARS3D is performed for a shallow water basin example: Etang de Berre.

Brief description of the different approaches

Let us to briefly describe the essence of each of the techniques and then perform a comparative analysis with concrete examples.

First model based on Navier-Stokes equations

For the first model, we consider the following Navier - Stokes equations [1,2]:

$$u_t' + uu_x' + vu_y' + wu_z' = -\frac{1}{\rho}a_x' + \left(\mu u_x'\right)_x' + \left(\mu u_y'\right)_y' + \left(\nu u_z'\right)_z' + 2\Omega(v\sin\theta - w\cos\theta), \quad (1)$$

$$v_t' + uv_x' + vv_y' + wv_z' = -\frac{1}{\rho}a_y' + \left(\mu v_x'\right)_x' + \left(\mu v_y'\right)_y' + \left(\nu v_z'\right)_z' - 2\Omega u\sin\theta, \quad (2)$$

$$w_t' + uw_x' + vw_y' + ww_z' = -\frac{1}{\rho}a_z' + \left(\mu w_x'\right)_x' + \left(\mu w_y'\right)_y' + \left(\nu w_z'\right)_z' + 2\Omega u\cos\theta, \quad (3)$$

and the equation of continuity for incompressible fluid: $u_x' + v_y' + w_z' = 0$, (4), where $\mathbf{V} = \{u, v, w\}$ – components of a vector of velocity, $\boldsymbol{a}$ – hydrostatic pressure, $\boldsymbol{\rho}$ – density, $\boldsymbol{\Omega}$ – angle velocity of the Earth rotation, $\boldsymbol{\theta}$ – angle between a vector of angle velocity and normal vector, $\boldsymbol{\mu, \nu}$ – horizontal and vertical components of the coefficient of turbulent exchange.

For conservative difference scheme based on the natural balance equations written for elementary volume (cell) grid area. Entering the balance equations derivatives and integrals should be replaced by approximate difference expressions. As a result, we obtain an homogeneous difference schemes. This method of obtaining conservative schemes is called integral-interpolation method.

An effective numerical method for solving problems of hydrodynamics is the SOR - method. We consider the variant of this method, known as method of pressure correction. This method is an additive scheme of splitting into physical processes and guarantees the mass balance (equation of continuity). Consider the system of equations on the physical processes.

Split each equation of system into two parts as follows:

$$\frac{\tilde{u} - u}{\tau} + u\tilde{u}_x' + v\tilde{u}_y' + w\tilde{u}_z' = \left(\mu\tilde{u}_x'\right)_x' + \left(\mu\tilde{u}_y'\right)_y' + \left(\nu\tilde{u}_z'\right)_z' + 2\Omega(v\sin\theta - w\cos\theta), \quad (5)$$

$$\frac{\tilde{v} - v}{\tau} + u\tilde{v}_x' + v\tilde{v}_y' + w\tilde{v}_z' = \left(\mu\tilde{v}_x'\right)_x' + \left(\mu\tilde{v}_y'\right)_y' + \left(\nu\tilde{v}_z'\right)_z' - 2\Omega u\sin\theta, \quad (6)$$

$$\frac{\tilde{w} - w}{\tau} + u\tilde{w}_x' + v\tilde{w}_y' + w\tilde{w}_z' = \left(\mu\tilde{w}_x'\right)_x' + \left(\mu\tilde{w}_y'\right)_y' + \left(\nu\tilde{w}_z'\right)_z' + 2\Omega u\cos\theta, \quad (7)$$

$$\frac{\overline{u} - \tilde{u}}{\tau} = -\frac{1}{\rho}a_x', \frac{\overline{v} - \tilde{v}}{\tau} = -\frac{1}{\rho}a_y', \frac{\overline{w} - \tilde{w}}{\tau} = -\frac{1}{\rho}a_z'. \quad (8)\text{-}(10)$$

where u - value at the previous temporary layer, $\overline{u}$ – at the current time layer, $\tilde{u}$ – for non interim temporary layer.

After differential of equations (8) - (10) on variables x, y, z respectively and summarizing and including (4) as a result we received:

$$a_{xx}'' + a_{yy}'' + a_{zz}'' = \frac{\rho}{\tau}\left(\tilde{u}_x' + \tilde{v}_y' + \tilde{w}_z'\right) \quad (11)$$

Equations (5)-(10), (11) are solved by the SOR method.

In the system of equations (5) - (10), (11) instead of partial derivatives, we will use their finite-difference analogues, obtained by means of integral-interpolation method. The most cumbersome task is to calculate the pressure presented by the Poisson equation. Finite-difference analogs of equations (5) - (10), (11) are solved by alternate - triangle method of rapid descent [3]. The main advantage of these schemes - a wide margin of stability. Discrete model is also conveniently used to calculate the stationary currents.

Second model based on Boltzmann equation

The second approach is based on the continuous Boltzmann equation - integral-differential equations, which describes the evolution of one particle distribution function f (x, ξ, t) in momentum space:

$$\frac{\partial f}{\partial t}+\boldsymbol{\xi}\cdot\nabla_{\mathbf{x}} f+\mathbf{a}\cdot\nabla_{\boldsymbol{\xi}} f=Q(f,f), \tag{12}$$

where $Q(f,f)$ - collision integral. The situation in the physical space x and the speed indicated in the space of momentum (or velocity) is indicated $\boldsymbol{\xi}$. Term $f(\mathbf{x},\boldsymbol{\xi},t)d^3x\,d^3\xi$ represents the probability of finding the particle in the volume d^3x around the *x* and at velocities between ξ and $\xi + d\xi$, *a* - the force per unit mass acting on a particle.

In numerical solution of the Boltzmann equation using Lattice Boltzmann Method (LBM), which uses minimal discrete kinetic model for solving problems in fluid mechanics and other fields of physics [5-8]. Instead of a direct solution of Navier-Stokes equations, LBM includes the lattice Boltzmann equation (LBE), which describes the evaluation of the distribution of an ensemble of particles on a lattice, the collective behavior that asymptotically represents the dynamics of fluid flow. As shown in dealing with LBE in the limit of fluid flow is produced to the weakly compressible Navier-Stokes equations.

The effects of particle collisions in determining LBE generally represent a relaxation model. One of the most common - is the single relaxation time model (SRT), also known as the BGK (Bhatnagar, Gross and Krook) model [12]. Generalized Lattice Boltzmann Equation (GLBE) with external forces consists of the evolution equation for the distribution function of particle populations as they move and collide on a lattice and is given by [16, 17]:

$$f_\alpha\left(\vec{x}+\vec{e}_\alpha\delta_t,t+\delta_t\right)-f_\alpha\left(\vec{x},t\right)=-\sum_\beta\Lambda_{\alpha\beta}\left(f_\beta-f_\beta^{eq}\right)+\sum_\beta\left(I_{\alpha\beta}-\frac{1}{2}\Lambda_{\alpha\beta}\right)S_\beta\delta_t. \tag{13}$$

Here the left side of equation (13) corresponds to a change of the distribution function for the interval δ_t, so the ensemble of particles moving from the situation $\vec{x}$ in its neighboring position $\vec{x}+\vec{e}_\alpha\delta_t$ with the speed along the characteristic directions. We consider the three-dimensional 19-speed $\vec{e}_\alpha$ and a lot of velocity of particles (D3Q19), shown in Fig.1, with the following:

$$\vec{e}_\alpha=\begin{cases}(0,0,0) & \alpha=0\\ (\pm c_x,0,0),(0,\pm c_y,0),(0,0,\pm c_z) & \alpha=1,..,6\\ (\pm c_x,\pm c_y,0),(\pm c_x,0,\pm c_z),(0,\pm c_y,\pm c_z) & \alpha=7,..,18\end{cases} \tag{14}$$

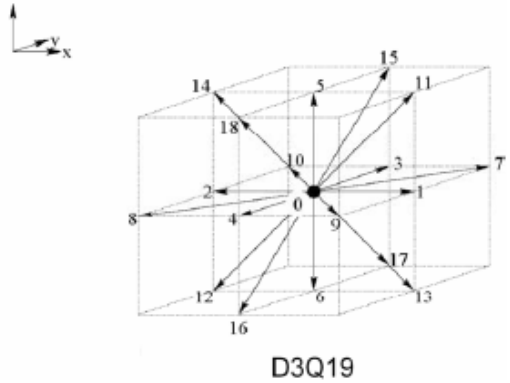

D3Q19

FIG. 1 – Velocities of particles (D3Q19)

Values of velocity components c_x,c_y,c_z of a particle $\vec{e}_\alpha$ are determining $c_x=\delta_x/\delta_t$, $c_y=\delta_y/\delta_t$ and $c_z=\delta_z/\delta_t$, where $\delta_x,\delta_y,\delta_z$ – grid steps in space, also δ_t – time step. The first term on the right side of

equation (13) represents the cumulative effect of particle collisions in the evolution of the distribution function f_α. GLBE has a general form of a matrix with multiple collisions of relaxation times that correspond to the basic physical parameters such as density, momentum and stress tensor. They, in turn, represent different points of kinetic distribution function. The second term on the right side of equation (13) changes in the distribution function dependent on external fields of forces $\vec{F}$ through source - S_α , $I_{\alpha\beta}$ – elements of the unit matrix. The source can be written as follows [13,11]: $S_\alpha = \frac{\left(e_{\alpha j} - u_j\right)F_j}{\rho c_s^2} f_\alpha^{eq,M}\left(\rho,\vec{u}\right)$, where

$$f_\alpha^{eq,M}\left(\rho,\vec{u}\right) = \omega_\alpha \rho\left\{1+\frac{\vec{e}_\alpha\cdot\vec{u}}{c_s^2}+\frac{\left(\vec{e}_\alpha\cdot\vec{u}\right)^2}{2c_s^4}-\frac{\left(\vec{u}\cdot\vec{u}\right)}{2c_s^2}\right\}, \omega_\alpha = \begin{cases} 1/3 & \alpha = 0 \\ 1/18 & \alpha = 1,..,6 \\ 1/36 & \alpha = 7,..,18 \end{cases}, \tag{15}$$

and $c_s = \sqrt{c_x^2 + c_y^2 + c_z^2}/3$ – speed of sound of model, F_j – cartesian components of external force.

The local macroscopic density and velocity are calculated as follows: $\rho = \sum_\alpha f_\alpha$, $\vec{j} \equiv \rho\vec{u} = \sum_\alpha f_\alpha \vec{e}_\alpha + \frac{1}{2}\vec{F}\delta_t$, and pressure p can be found as $p = \rho c_s^2$.

The nature of the kinetic equation (13), and in particular, the matrix of the collision $\Lambda_{\alpha\beta}$ becomes more evident when we define it in terms of sets of linearly independent moments $\hat{\mathbf{f}}$ and $\hat{\mathbf{S}}$, instead of the functions assigned $\mathbf{f} = \left[f_0, f_1, ..., f_{18}\right]^T$ and $\mathbf{S} = \left[S_0, S_1, S_2, ..., S_{18}\right]^T$, ie through $\hat{\mathbf{f}} = \left[\hat{f}_0, \hat{f}_1, ..., \hat{f}_{18}\right]^T$ and $\hat{\mathbf{S}} = \left[\hat{S}_0, \hat{S}_1, \hat{S}_2, ..., \hat{S}_{18}\right]^T$, which is obtained through a matrix transformation $T: \hat{\mathbf{f}} = T\mathbf{f}$, $\hat{\mathbf{S}} = T\mathbf{S}$. Elements of the matrix T are given in [16]. Each row of matrix is orthogonal to any other series. This matrix Λ is such that the matrix of collisions becomes a diagonal matrix $\hat{\Lambda} = diag(s_0, s_1, s_2, ..., s_{18})$, where $s_0, s_1, s_2, ..., s_{18}$ relaxation time the coefficients of the relevant moments, after transformation $\hat{\Lambda} = T\Lambda T^{-1}$.

Described two approaches were adopted for a shallow water basin Etang de Berre (see Fig.3), also results of modeling were compared with results of simulation using a package Mars3D (IFREMER).

Thus, in the three-dimensional domain of definition of the problem $G = \{(x,y,z): H(x,y) \le z \le 0\}$ - shallow basin Etang de Berre, is required to find the components of flow velocity $u = u(x,y,z,t)$, $v = v(x,y,z,t)$, $w = w(x,y,z,t)$, pressure of water $P = P(x,y,z,t)$, where $H(x,y)$ the known function of the bottom topography. External forces in this model are: wind force, the force of friction on the bottom and the Coriolis force.

Boundary conditions on the free surface is thus: $w = 0, \nu\frac{\partial u}{\partial z} = F_{sx}(x,y,t), \nu\frac{\partial v}{\partial z} = F_{sy}(x,y,t), \frac{\partial p}{\partial z} = 0$, where $\mathbf{F}_s = F_{sx}\mathbf{i} + F_{sy}\mathbf{j} = \theta\rho_a|\mathbf{w}|\mathbf{w}$ – the friction force of wind on the sea surface, where $\theta = 8.8\cdot 10^{-3}$ - coefficient of friction on the sea surface, $\rho_a = 1,25$ - the density of the atmosphere, $\mathbf{w}$ - wind speed (Law Van Dorn). These conditions for the velocity, consistent with the boundary condition for the particle distribution function: $f_\alpha(x,y,0,t) = f_\alpha(x,y,-\delta_z,t) + \delta_z\omega_\alpha\rho\frac{(\mathbf{e}_\alpha\cdot\mathbf{F}_s)}{\nu c_s^2}$.

At the bottom $z = H(x,y)$ and on the solid parts of the boundary no slip conditions are applied to the velocity of adhesion $u = v = w = 0$ and pressure conditions $\frac{\partial p}{\partial n} = 0$ that correspond to the bounce-back boundary condition (BB BC) for the distribution function: $f_{\bar{\alpha}} = f_\alpha$.

Also, such conditions can be used at the bottom:

$\nu\frac{\partial u}{\partial z}=-F_{bx}(x,y,t),\ \nu\frac{\partial v}{\partial z}=-F_{by}(x,y,t),\nu\frac{\partial w}{\partial z}=-F_{bz}(x,y,t),$ where $\mathbf{F}_b=F_{bx}\mathbf{i}+F_{by}\mathbf{j}+F_{bz}\mathbf{k}=\theta_1\rho_0|\mathbf{w}|\mathbf{w}$ – the friction force of water on the surface of the bottom, where $\theta_1=1.3\cdot10^{-6}$ - coefficient of friction on the bottom, ρ_0 - the density of water, $\mathbf{W}$ - the speed of flow. The corresponding boundary condition for the particle distribution function: $f_\alpha(x,y,H(x,y),t)=f_\alpha(x,y,H(x,y)+\delta_z,t)+\delta_z\omega_\alpha\rho\frac{(\mathbf{e}_\alpha\cdot\mathbf{F}_b)}{\nu c_s^2}$.

At the liquid part of the border and in the sources (estuarine) $\vec{u}=\vec{u}_{const}$ set the known flow of liquid. For this type of boundary conditions for the components of the velocity at the border, often using BB BC [8,9] for the partial distribution function f_α at the entrance: $f_{\bar{\alpha}}=f_\alpha+2\omega_\alpha\rho\frac{(\mathbf{e}_{\bar{\alpha}}\cdot\mathbf{u})}{c_s^2}$, where $\mathbf{e}_\alpha$ and $\mathbf{e}_{\bar{\alpha}}$ denote the opposite directions of each other: $\mathbf{e}_\alpha=-\mathbf{e}_{\bar{\alpha}}$.

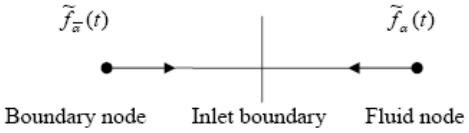

FIG. 2 – Location of boundaries in the entrance.

Boundary conditions.

For the open boundary: $\vec{u}_n=\vec{u}(t),\ \left(|\vec{u}_n|\approx1\ m/s\right)$ - in the general case a function of time (direction of velocity can still depend on the ebb tide or during a given period of time)

For rivers: $\vec{u}_n=\vec{u}_0,$ estuaries l'Arc and the la Touloubre, where the set-known flow of liquid.

Connection between Etangs de Berre and de Bolmon: $\frac{\partial\mathbf{u}}{\partial\mathbf{n}}=0$, where n - normal to the side of the Berre.

On moving the marine environment at all times act Coriolis force, calculated as follows: $\vec{F}_{cor}=2\rho\left[\vec{\Omega}\times\vec{u}\right]$,where $\vec{\Omega}$ – vector angular velocity of rotation of the earth.

Numerical results and comparison

Briefly describe the essence of each of the techniques and then perform a comparative analysis. Numerical simulation results using the Lattice Boltzmann method are presented in Fig.3 (a), for the next set of parameters: Ma = 0.002, Re = 10, northern wind (5 m / s). Similar results for the reservoir with the same wind speed, calculated by the amendments to the pressure are illustrated in Fig.3 (b). For comparison, results obtained using Mars 3D [18, 20] are also depicted in Fig.3. To the north-west wind (5 m / c), taking into account the effect of tidal-drip caps in the channel Caronte. Simulation results for all three models agree qualitatively with each other, however, LBM - approach was more promising in terms of existence and uniqueness of solutions with well-developed turbulence.

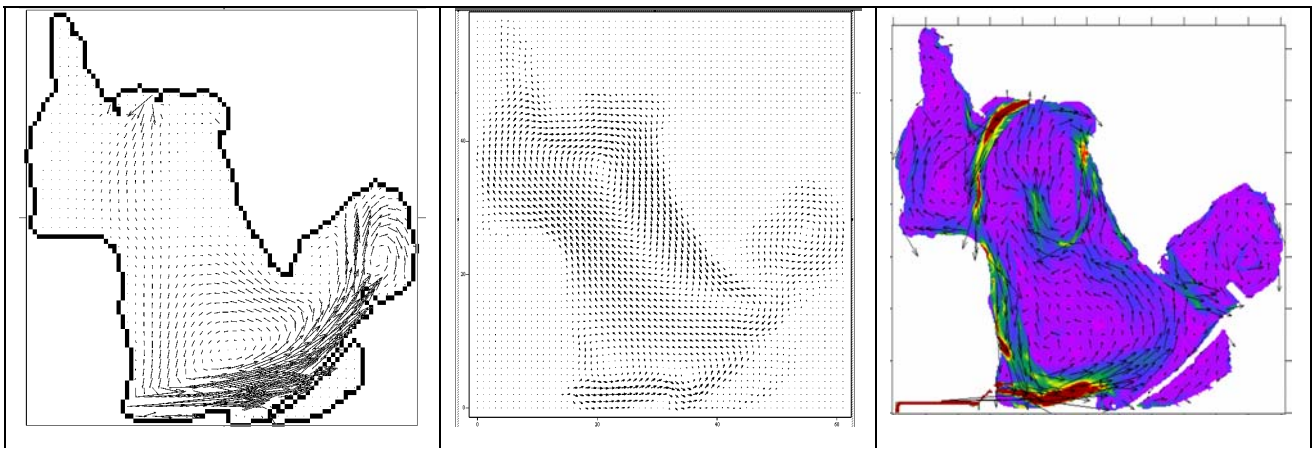

(a) *(b)* *(c)*

FIG. 3 – Barotropic currents: (a) LBM, (b) Azov 3D, (c) Mars 3D.

References

[1] Marchuk G.I., Sarkisyan A.S. Mathematical modeling of ocean circulation.- M.: Nauka. 1988.-304 p.

[2] Rouch P. Computative hydrodynamics: Transl from Eng. – M.: Mir,1980.- 616 p.

[3] Konovalov A.N. Theory of alternative-triangle method. Sibirskii matematicheskii zhurnal, 2002, 43:3, 552-572

[4] Belotserkovskii A.N., Oparin A.M., Chechetkin V. M. Turbulence. New approaches. Moscow, Nauka, 2002.

[5] Chen S. and G. Doolen, Ann. Rev. Fluid Mech. 8, 2527 (1998).

[6] Succi S., The Lattice Boltzmann Equation for Fluid Dynamics and Beyond (Clarendon Press, Oxford, 2001).

[7] Succi S., I. Karlin, and H. Chen, Rev. Mod. Phys. 74, 1203 (2002).

[8] Yu D., R. Mei, L.-S. Luo, and W. Shyy, Prog. Aero. Sci. 39, 329 (2003).

[9] McNamara G. and G. Zanetti, Phys. Rev. Lett. 61, 2332 (1988).

[10] Higuera F. and J. Jimenez, Europhys. Lett. 9, 663 (1989).

[11] Higuera F., S. Succi, and R. Benzi, Europhys. Lett. 9, 345 (1989).

[12] Bhatnagar P., E. Gross, and M. Krook, Phys. Rev. 94, 511 (1954).

[13] Lallemand P. and L.-S. Luo, Phys. Rev. E 61, 6546 (2000).

[14] Benzi R., S. Succi, and M. Vergassola, Phys. Rept. 222, 145 (1992).

[15] Resibois P. and M. D. Leener, Classical Kinetic Theory of Fluids (John Wiley and Sons, New York, 1977).

[16] d`Humieres D., I. Ginzburg, M. Krafczyk, P. Lallemand, and L.-S. Luo, Phil. Trans. R. Soc. Lond. A 360, 437 (2002).

[17] Premnath K. N. and J. Abraham, J. Comput. Phys. 224, 539 (2007).

[18] User manual Mars 3D v.7.34, IFREMER , 2007.

[19] Lazure P., Dumas F., 2008. An external-internal mode coupling for a 3D hydrodynamical model at regional scale (MARS). Adv. Wat. Res., 31, 233-250.

[20] Fiandrino A., Martin Y., Got P., Bonnefont J.L., Troussellier M., 2003. Bacterial contamination of Mediterranean coastal seawater as affected by riverine inputs: simulation approach applied to a shellfish breeding area (Thau lagoon, France). Water Res. 37, 1711-1722.